Sensors and Materials, Vol. 36, No. 8 (2024) 3595–3607
MYU Tokyo

S & M 3752

Achievement of Hierarchical Optimization Planning for Distributed Generation Network Based on Improved Sand Cat Swarm Optimization

Liying Zhou[1] and Hsiung-Cheng Lin[2*]

[1]College of Mechanical and Electrical Engineering, Jinling Institute of Technology, Nanjing 211199, China
[2]Department of Electronic Engineering, National Chin-Yi University of Technology, Taichung 41170, Taiwan

(Received November 17, 2023; accepted April 18, 2024)

Keywords: distribution network, distributed generation, uncertainty, improved sand cat swarm optimization algorithm, DG hierarchical planning model

The penetration of renewable energy resources for distribution networks can significantly impact the security of power supply systems. To improve the penetration efficiency, a hierarchical optimization planning for a distributed generation (DG) network using the improved sand cat swarm optimization (ISCSO) is proposed to determine the optimal location and capacity of DG into the distribution network. Firstly, the sensor is used to collect data, and the ISCSO algorithm is used to construct a complex nonlinear DG planning problem, thus reducing the impact of DG uncertainty. Second, a DG hierarchical planning model is established to select the optimal location and capacity of DG access to the distribution network. Finally, in the classical test system, the effectiveness of the proposed model is verified by setting up multiple cases. The test results confirm that the total annual cost and power loss of the DG system can be reduced by 13.1 and 40.5%, respectively.

1. Introduction

The continuous growth of the world's population has led to an increase in global energy consumption. Owing to limited fossil energy resources on Earth, this contradiction has significantly intensified in recent years.(1) On the other hand, renewable energy is inexhaustible and easy to obtain, and causes little environmental pollution.(2) The representative renewable energy power generation systems include wind turbine (WT) and photovoltaic (PV) cells.(3) The penetration rate of renewable energy in the power grid is thus increasing.(4,5) As a result, the distributed generation (DG) can provide a better solution for renewable energy sources in achieving sustainable development.(6–8)

DG is superior in terms of low carbon emission, flexible control, and low investment cost, but its grid-connected operation would increase the grid complexity and uncertainty.(9) Planning in distribution networks reasonably can effectively improve the power-flow distribution and node voltage quality, and reduce network losses. In contrast, problems such as increased losses and

*Corresponding author: e-mail: hclin@ncut.edu.tw
https://doi.org/10.18494/SAM4785

ISSN 0914-4935
https://myukk.org/

the decreased quality of voltage may occur from time to time. To consider the economy of the system and uncertainty in DG output, a DG planning model with an annual total cost should be established. The core content of DG planning research is mainly focused on two aspects: site selection and capacity determination.[10,11] Classical methods for these aspects include particle swarm optimization [12] and the cuckoo algorithm.[13] Uniyal and Sarangi [14] took into account the time-varying load of the distribution network. On the basis of enhancing a traditional whale optimization algorithm, an adaptive whale optimization algorithm was proposed to allocate DG to the actual distribution network. The feasibility was verified by the simulation analyses of 69-node and 129-node systems. Compared with some previous approaches, the network loss in the system could be reduced more significantly. Sellami *et al.* [15] introduced an improved method to reasonably determine the capacity and location of DG, where it combined with the MOPSO algorithm and Matpower software toolbox. Ali *et al.* [16] improved the wild horse optimization algorithm for solving the DG planning problem using benchmark functions. Experiments showed that it could effectively improve the voltage distribution and therefore enhance the economy of the system in the complex DG configuration problem.

Cikan and Cikan [17] attempted to minimize the system loss using the balanced optimization algorithm integrated with DG to the 123-node distribution network, and the performance of the model was verified by comparative analysis. Gümüş *et al.* [18] proposed a stability index based on the Thevenin theorem, taking into consideration voltage deviation and network loss. The optimal DG allocation and sizing in distribution systems were verified using the 69-node and 188-node systems. Gao *et al.* [19] developed a DG multi-objective programming model that described the spatial and temporal correlations of loads. By introducing the principle of economic consumption, Sun *et al.* [20] reported a DG planning model to reach a fast solution by measuring curtailing light and wind in the steady-state security region. The effectiveness of the proposed model was proved by the simulation performance.

2. Model Description

2.1 Sensor-based uncertainty handling

In this study, WT and PV were applied in DG systems. We assumed that both WT and PV units adopt constant power control, but the output power is random and intermittent. All data were collected from wind speed [21], temperature, and light sensors [22] during a one-year period of time. The K-means algorithm was used to select the application scenarios in each season.[23] Four scenarios were classified: spring, summer, autumn, and winter days. Finally, the typical wind speed and light intensity of each season can be converted into the output of WT and PV.

2.2 Objective function

The optimization goal is the total annual cost F.

$$F = f_{total} = f_l + f_{om} + f_{loss} + f_{en} \tag{1}$$

2.2.1 DG investment cost f_l

$$f_l = \frac{\alpha(1+\alpha)^y}{(1+\alpha)^y - 1} \times \left[\sum_{i=1}^{n} \left(c_{pv,l} P_{pv,i} \right) + \sum_{i=1}^{n} \left(c_{wt,l} P_{wt,i} \right) \right] \tag{2}$$

Here, n is the number of nodes in the system to be installed for DG, $P_{wt,i}$ and $P_{pv,i}$ are the rated capacities of WT and PV installed in the i_{th} node, and $c_{wt,l}$ and $c_{pv,l}$ are the unit capacity investment costs of WT and PV, respectively. For the investment conversion ratio, α is the maximum number of years of distributed power operation.

2.2.2 DG operating cost f_{om}

$$f_{om} = \sum_{p=1}^{n_p} \sum_{i=1}^{n} t_p \left(c_{pv,om} P_{pv,i,p} + c_{wt,om} P_{wt,i,p} \right) \tag{3}$$

Here, $P_{wt,i,p}$ and $P_{pv,i,p}$ are the actual active power output of WT and PV installed using the i_{th} node under scenario p, respectively. $c_{wt,om}$ and $c_{pv,om}$ are the operating costs required for WT and PV to emit unit power, respectively. n_p is the number of simulated scenarios and t_p is the number of running days in scenario p.

2.2.3 Power purchase cost from superior power grid C_{en}

$$C_{en} = \sum_{s=1}^{N_s} \sum_{t=1}^{24} d_{p,t} P_{en,p,t} t_p \tag{4}$$

Here, $P_{en,p,t.}$ and $d_{p,t}$ are the active power and real-time electricity price purchased from the superior power grid at time t of scenario p, respectively.

2.2.4 Network loss cost f_{loss}

$$f_{loss} = \sum_{i=1}^{n_p} c_{loss} P_{loss,p} t_s \tag{5}$$

Here, $P_{loss,p}$ represents the total active power loss under scenario p and c_{loss} is the cost of active power loss per unit of electricity.

2.3 Objective function

2.3.1 DG installed capacity constraints

$$\begin{cases} 0 \le P_{i,DG} \le P_{i,DG,max} \\ 0 \le P_{i,wt} \le P_{i,wt,max} \\ 0 \le P_{i,pv} \le P_{i,pv,max} \end{cases} \tag{6}$$

Here, $P_{i,DG,\max}$ represents the maximum capacity of DG installed at node i, and $P_{i,wt,\max}$ and $P_{i,pv,\max}$ represent the maximum capacities of WT and PV at node i, respectively.

2.3.2 Node voltage constraints

$$U_{i,min} \le U_i \le U_{i,max} \tag{7}$$

Here, U_i is the voltage at node i. $U_{i,\min}$ and $U_{i,\max}$ are the minimum and maximum node voltages, respectively.

2.3.3 Power balance constraints

$$\begin{cases} U_{i,p}\sum_{i=1}^{N_n} U_{j,p}\left(G_{ij}\cos\varphi_{ij,p} + B_{ij}\sin\varphi_{ij,p}\right) = P_{i,p} \\ U_{i,p}\sum_{i=1}^{N_n} U_{j,p}\left(G_{ij}\sin\varphi_{ij,p} - B_{ij}\cos\varphi_{ij,p}\right) = Q_{i,p} \end{cases} \tag{8}$$

Here, $P_{i,p}$ and $Q_{i,p}$ represent the active power and reactive power flowing into node i at scenario p, respectively. $U_{i,p}$ and $U_{j,p}$ denote the voltage amplitudes of nodes i and j at scenario p, respectively. G_{ij} and B_{ij} represent the real and imaginary parts of the admittance between nodes i and j, respectively, and $\varphi_{ij,p}$ represents the impedance angle.

2.3.4 DG operation constraints

$$\begin{cases} 0 \le \delta_{i,DG} \le \delta_{i,max}^{DG} \\ \left(1-\delta_{i,DG}\right)P_{i,p,max}^{DG} \le P_{i,p}^{DG} \le P_{i,p,max}^{DG} \end{cases} \tag{9}$$

Here, the types of DG are WT and PV, and $P_{i,p,max}^{DG}$ is the upper limit of the active power output of DG installed in scenario p at node i. $\delta_{i,DG}$ and $\delta_{i,max}^{DG}$ are the active power reduction rate of DG and its maximum value, respectively.

2.4 Model transformation

On the basis of the principle of hierarchical coordination, the optimal planning scheme of DG was selected, and the total operation cost of DG in one year was considered. The layered model architecture is shown in Fig. 1, where the upper and lower layers have independent objective functions and constraints. The upper layer is used to determine the type, location, and capacity of DG. The optimization objective is the total annual cost, and the constraints are the installation capacity and permeability constraints of DG. The lower layer is the optimization subproblem of the distribution network in each scenario. The objective function is the total operating cost of DG, where the constraints are system, power flow, and DG operation constraints. The upper layer transfers the planning scheme of DG to the lower layer. After receiving the scheme, the lower layer calculates the total operation cost of DG, transmits the calculation results to the upper layer, where these results are used to calculate the objective function of the upper layer, and iterates to the maximum number of iterations. The above process is repeated until the maximum number of iterations is reached.

3. Sand Cat Swarm Optimization Algorithm (SCSO) and Its Improvement

3.1 Sand cat swarm optimization (SCSO) algorithm

In this study, the initialization method combining tent mapping and the Sobol sequence is applied to generate a more evenly distributed initial solution, which can considerably increase the performance and optimization speed of the algorithm. Then, we add the adaptive factor to

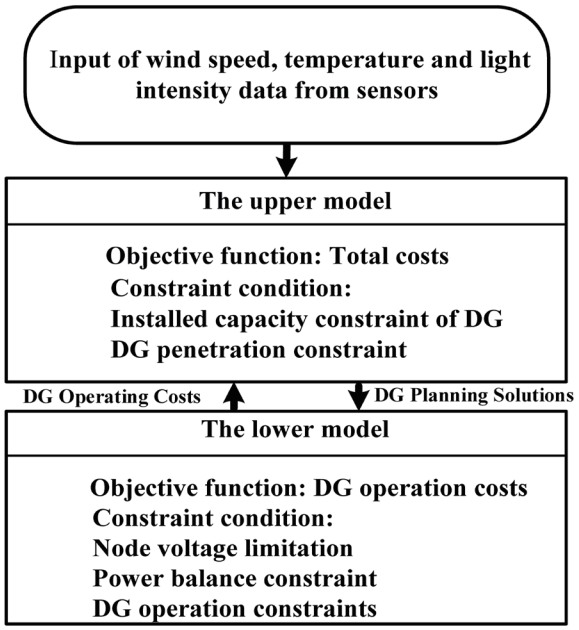

Fig. 1. Layered model architecture.

the update formula of the SCSO algorithm. The value of the adaptive factor can change with the iteration, so that the performance of the algorithm can be improved and the optimal solution can be found more rapidly.

In SCSO, the position of each sand cat represents a candidate solution to the problem. The strategy of searching for prey simulates the sand cat's search for prey, which mainly relies on its sensitive hearing and ability to perceive low-frequency sounds. The sand cat's location update formula is

$$\overrightarrow{r_G} = l_M - \left(\frac{2 \times L_M \times Iter_c}{Iter_{max} + Iter_{max}} \right), \tag{10}$$

$$RJ = 2 \times \overrightarrow{r_G} \times R_a - \overrightarrow{r_G}, \tag{11}$$

$$\overrightarrow{P}(t+1) = \overrightarrow{r_G} \times \left(\overrightarrow{P_b}(t) - R_a \times \overrightarrow{P_c}(t) \right) \times R_a, \tag{12}$$

where r_G is a low-frequency sensing parameter. *Ra* is a random number between 0 and 1. L_M is the parameter for simulating the hearing of sand cats, where $Iter_c$ and $Iter_{max}$ are the current and maximal iterations, respectively. *RJ* is the parameter for determining the two-stage switching between searching prey and attacking prey. $\overrightarrow{P_c}(t)$ is the best position of the sand cat and $\overrightarrow{P_b}(t)$ is the position of a random sand cat at the current number of iterations.

After searching for prey, the sand cat approaches the prey using its sensitive hearing. The position update formula of the sand cat attacking prey is expressed as

$$\overrightarrow{P_{rnd}} = \left| R_a \cdot \overrightarrow{P_b}(t) - \overrightarrow{P_c}(t) \right|, \tag{13}$$

$$\overrightarrow{P}(t+1) = \overrightarrow{P_b}(t) - \overrightarrow{r_G} \times R_a \times \overrightarrow{P}_{rnd} \times \cos(\alpha). \tag{14}$$

By combining the two stages, the formula for simulating the predation process of sand cats is expressed as

$$\begin{cases} \overrightarrow{P}(t+1) = \overrightarrow{r_G} \times \left(\overrightarrow{P_b}(t) - R_a \times \overrightarrow{P_c}(t) \right) \times rand(0,1) & |RJ| \le 1 \\ \overrightarrow{P}(t+1) = \overrightarrow{P_b}(t) - \overrightarrow{r_G} \times R_a \times \overrightarrow{P}_{rnd} \times \cos(\alpha) & |RJ| > 1 \end{cases}. \tag{15}$$

3.2 Improved sand cat swarm optimization (ISCSO) algorithm

3.2.1 Improvement of population position initialization

The distribution of the initial population generated by the SCSO algorithm is uneven and random. It combines tent mapping and Sobol sequence methods to perform the algorithm initialization process. Its form is expressed as

$$\vec{P}(t+1)=\begin{cases}\vec{P}(t)/\mu & x_T\in[0,\mu]\\ \left(1-\vec{P}(t)\right)/(1-\mu) & x_T\in(\mu,1]\end{cases}, \tag{16}$$

where μ is the boundary constant with the value of 0.3.

3.2.2 Dynamic self-adaptive factor

The adaptive factor is introduced into the position update formula of the sand cat. The global search ability of the algorithm is enhanced by the large weight in the early iteration, and the convergence speed is improved. The factor gradually decreases with the iteration, enhancing the algorithm's search ability and the accuracy of the solution. The weight formula is expressed as

$$w_1=0.5+0.5\cos\left(\frac{\pi}{2}\times\left(1-\frac{t}{T_{max}}\right)\right). \tag{17}$$

The position update formula of the sand cat after introducing the adaptive factor w_1 is

$$\begin{cases}\vec{P}=\overrightarrow{r_G}\times\left(\overrightarrow{w_1\times P_b}(t)-R_a\times\overrightarrow{P_c}(t)\right)\times R_a & |RJ|\le 1\\ \vec{P}=\overrightarrow{w_1\times P_b}(t)-\overrightarrow{r_G}\times R_a\times\vec{P}_{rnd}\times\cos(\alpha) & |RJ|>1\end{cases}. \tag{18}$$

When $|RJ| \le 1$, ISCSO uses the search position formula to update the position in the search phase; when $|RJ| > 1$, ISCSO is in the development phase, and the formula is applied to update the location.

3.2.3 Whale fall variation

The whale fall of the BWO algorithm simulates the death of individuals in the beluga whale population. The whale fall can remove the worst individuals in the population and generate an individual at a random position to maintain the balance of the number of individuals in the population. The whale fall is introduced as a population variation to SCSO to escape the local optimum. It is expressed as

$$\vec{P}(t+1)=r_1\overrightarrow{P_C}-r_2\overrightarrow{P_r}+r_3\overrightarrow{P_s}, \tag{19}$$

$$P_s=\left(u_b-l_b\right)e^{\left(-2\rho_f\times nT/T_{max}\right)}, \tag{20}$$

$$\rho_f=\frac{0.1-0.05Iter}{Iter_{max}}, \tag{21}$$

where r_1, r_2, and r_3 are random numbers, $\overrightarrow{P_r}$ is the position of a random sand cat, P_s is the step size of variation, u_b and l_b are the bounds of the variable, and ρ_f is the probability of variation.

3.3 Performance analysis of ISCSO algorithm

In this study, three measures were used to improve the SCSO algorithm, and the ISCSO algorithm was thus derived. Four benchmark functions including the single-peak and multipeak test functions were selected for the performance test, as shown in Table 1.

The test results using Matlab R2021b in the F1–F4 test are shown in Table 2. The number of iterations of each optimization algorithm is set as 500 times, and the number of populations is set as 30. Also, each test function runs 20 times. In the test results of unimodal test functions, the test results of the ISCSO algorithm are superior to those of the SCSO, PSO, GWO, and WOA algorithms, confirming the best optimization effect. In addition, its average and optimal values are closest to the optimal value of the test function. Also, the standard deviation of ISCSO in the results of the unimodal test function is the smallest, indicating the highest stability.

4. Case Analysis

The curves of wind speed and light intensity in four seasons obtained by K-means clustering are shown in Fig. 2. The wind speed and light intensity change with time. The difference between the wind speed and the light intensity in different seasons is obvious. The wind speed in winter and spring is higher, and the light intensity in spring and summer is higher.

Table 1
Benchmark test functions.

Function	Range	Optimization
$F_1(x)=\sum_{i-1}^{n}x_i^2$	[−100, 100]	0
$F_2(x)=\sum_{i=1}^{n}\lvert x_i\rvert+\prod_{i=1}^{n}\lvert x_i\rvert$	[−10, 10]	0
$F_3(x)=\frac{1}{10}\left\{\sum_{j=1}^{k}\left[1+\sin^2(3\pi x_j+1)\right]^2(x_j-1)^2(x_k-1)^2\left[1+\sin^2(2\pi x_k)\right]\right\}+\sum_{j=1}^{k}v(x_j,5,100,4)$	[−50, 50]	0
$F_4(x)=\sum_{i=1}^{11}\left[a_i-\frac{x_1\left(b_i^2+b_i x_2\right)}{b_i^2+b_i x_3+x_4}\right]^2$	[−5, 5]	0.0003

Table 2
Test results of benchmark functions.

Function	Algorithm	Average	Std	Best fitness	Worst fitness
$F(x_1)$	ISCSO	1.3972E−165	0	2.9254E−168	5.3965E−165
	SCSO	1.3989E−113	3.1252E−113	4.2559E−119	6.9896E−113
	WOA	2.3949E−70	3.8502E−70	1.6288E−72	9.2178E−70
	PSO	0.0212	0.0199	0.0065	0.5580
$F(x_2)$	ISCSO	3.5881E−85	7.8830E−85	2.0255E−89	1.7688E−84
	SCSO	5.1038E−61	1.0130E−60	1.0416E−64	2.3202E−60
	WOA	6.0277E−53	3.0600E−52	3.7024E−60	1.6876E−51
	PSO	16.4324	0.9043	14.7342	18.3365
$F(x_3)$	ISCSO	8.2961E−04	7.2222E−04	9.0405E−05	0.0018
	SCSO	2.4993	0.1309	2.3041	2.6329
	WOA	1.7073E+04	1.3726E+04	0.0135E+04	3.5566E+04
	PSO	2.1618	0.5057	1.4054	2.7595
$F(x_4)$	ISCSO	0.4185E−03	0.0972E−03	0.3076E−03	0.5211E−03
	SCSO	0.0007	0.0005	0.0003	0.0013
	WOA	0.7092E−03	0.0337E−03	0.6717E−03	0.7489E−03
	PSO	0.0011	3.2163E−04	8.2751E−04	0.0016

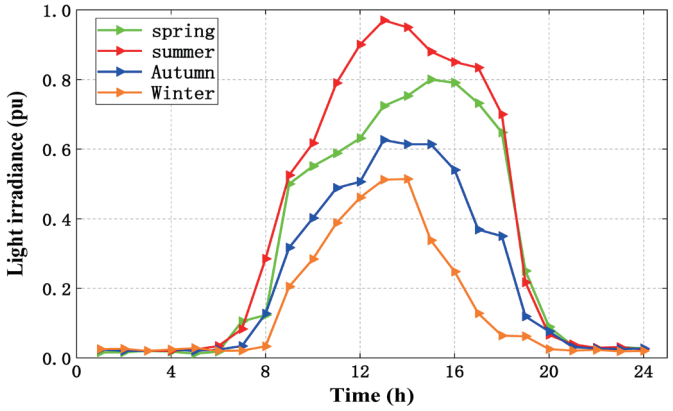

(a)

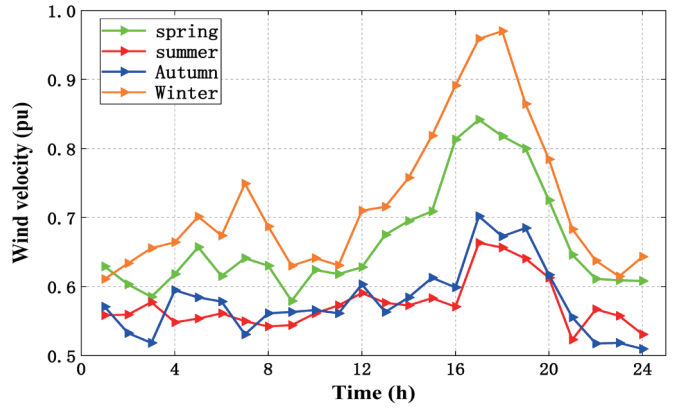

(b)

Fig. 2. (Color online) Seasonal wind speed and light intensity curve. (a) Intensity of illumination and (b) wind speed.

In this study, the IEEE33 system was selected to test the system. The total load of the system is 3715 + j2350 KVA. The reference voltage of the system is 12.66 kV, and other parameters are the default parameters of the IEEE33 system. The types of DG are WT and PV. Table 3 shows some parameters of WT and PV. The candidate access nodes of the WT access system are 12, 17, and 26, and the candidate access nodes of PV are 3, 7, and 28. The maximum DG capacities of the total system and the single node connected to the distribution network are 1800 and 800 kW, respectively.

A variety of algorithms, that is, the PSO, SCSO, and WOA algorithms, are selected for comparison with the ISCSO algorithm. The number of individuals in all algorithms is set to 50, and the number of iterations is 100. The iterative curves for the different algorithms are shown in Fig. 3.

The results obtained with the four algorithms are shown in Table 4 and reveal that the proposed ISCSO has the highest accuracy. Also, both the total annual cost and the objective function value are the smallest, presenting the highest economy.

Table3
Parameters of DGs.

	WT	PV
Investment cost ($/kWh)	855.9	966.3
Operating and maintenance cost ($/kWh)	0.03	0.03
Maximum useful life (year)	20	20
Present value coefficient	0.06	0.06

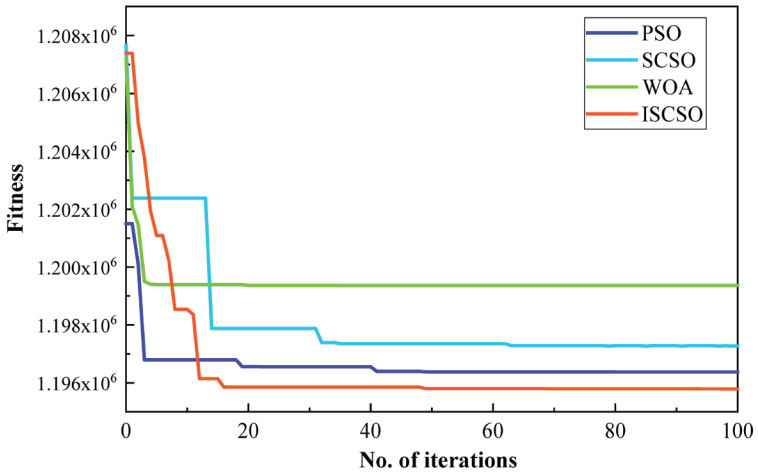

Fig. 3. (Color online) Convergence curves for different algorithms.

Table 4
Running results of different algorithms.

Algorithm	$\{WT\}^{bus}$ (kW)	$\{PV\}^{bus}$ (kW)	Cost ($)
PSO	$\{759\}^{12}\{240\}^{17}$	$\{317\}^{7}\{470\}^{28}$	1.191E−06
SCSO	$\{203\}^{12}\{795\}^{17}$	$\{800\}^{28}$	1.2064E−06
WOA	$\{692\}^{12}\{251\}^{17}$	$\{508\}^{7}\{348\}^{28}$	1.192E−06
ISCSO	$\{654\}^{12}\{345\}^{17}$	$\{800\}^{28}$	1.190E−06

The IEEE33 system is evaluated from the economic viewpoint, and the DG is planned. The smaller the annual comprehensive cost, the higher the economic benefit of the system. Two scenarios are set up to verify the effectiveness of the proposed model through comparative experiments.

Case 1: The initial system has no DG installed.

Case 2: The proposed model is used to install DG into the system.

The optimization results for the two scenarios are shown in Table 5. Compared with the initial Case 1, the total annual cost of Case 2 is reduced by 13.1%. The details of the cost of each case are shown in Table 6. In Case 1, most of the cost is that for purchasing electricity. In Case 2, the distribution network with DG shows increases in both investment and operation costs. On the other hand, the cost of purchasing electricity is considerably reduced by 33.5%, and the cost of active power loss is reduced by 40.2%.

Figure 4 shows the total voltage deviation in each node within one day in the summer scenario. Most of the node voltage deviations in Case 1 are large and some even exceed the limit.

Table 5
Operation results for the two cases.

Case	$\{WT\}^{bus}$ (kW)	$\{PV\}^{bus}$ (kW)	f_{total} ($)
Case 1	—	—	1.37E−06
Case 2	$\{654\}^{13}\{345\}^{17}$	$\{800\}^{27}$	1.19E−06

Table 6
Cost components of the two cases.

Case	Cost ($)			
	C_1	C_{om}	C_{en}	C_{loss}
Case 1	—	—	1.31 E−06	6.55 E−04
Case 2	7.45 E−04	2.05 E−05	8.71 E−05	3.92 E−04

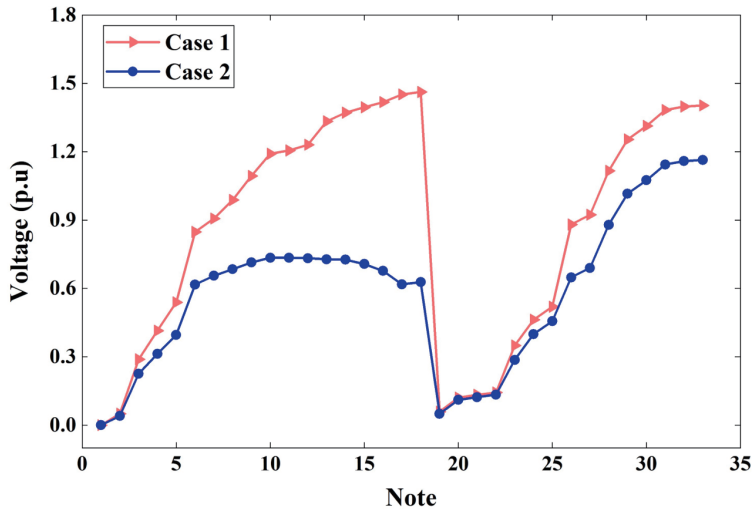

Fig. 4. (Color online) Total voltage deviation for the summer scenario in the two cases.

In Case 2, DG is installed so the total voltage deviation in most nodes decreases significantly. Figure 5 shows the 24 h active power loss in the summer scenario. Compared with the initial state without DG, the network loss in Case 2 is reduced every hour. In particular, between 8 and 17 h, the network loss is about half that without DG.

Three-dimensional diagrams of typical daily voltage distributions under various scenarios in summer are shown in Fig. 6. In Case 1, the voltage fluctuation is large and the overall power level is low. In Case 2, the difference between the highest and lowest node voltages is very small, and only a small part of the node voltage deviation exceeds the limit.

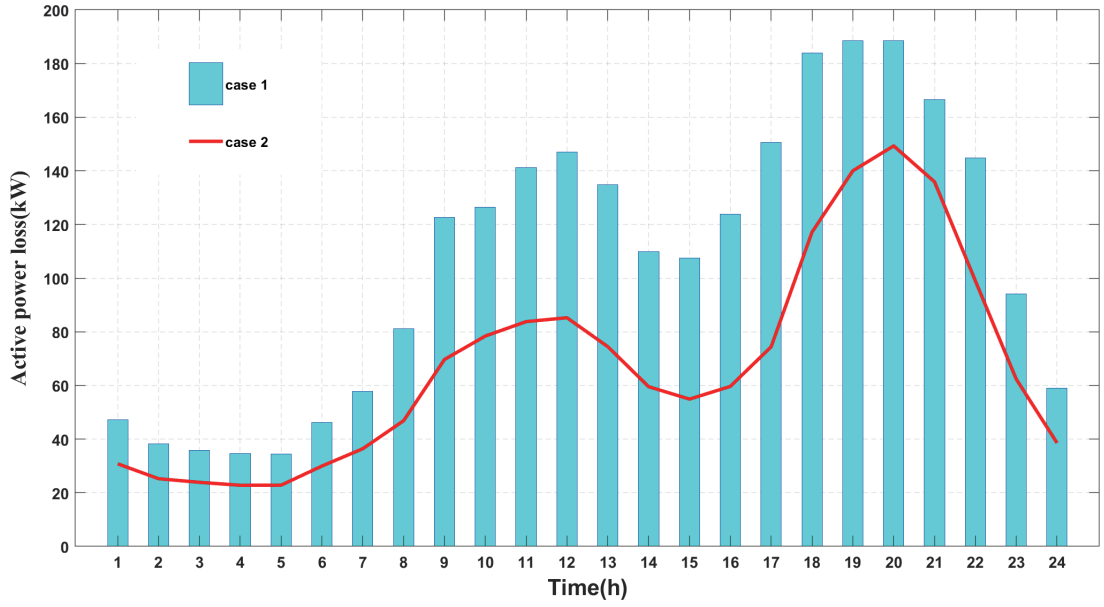

Fig. 5. (Color online) 24 h power loss in the two cases.

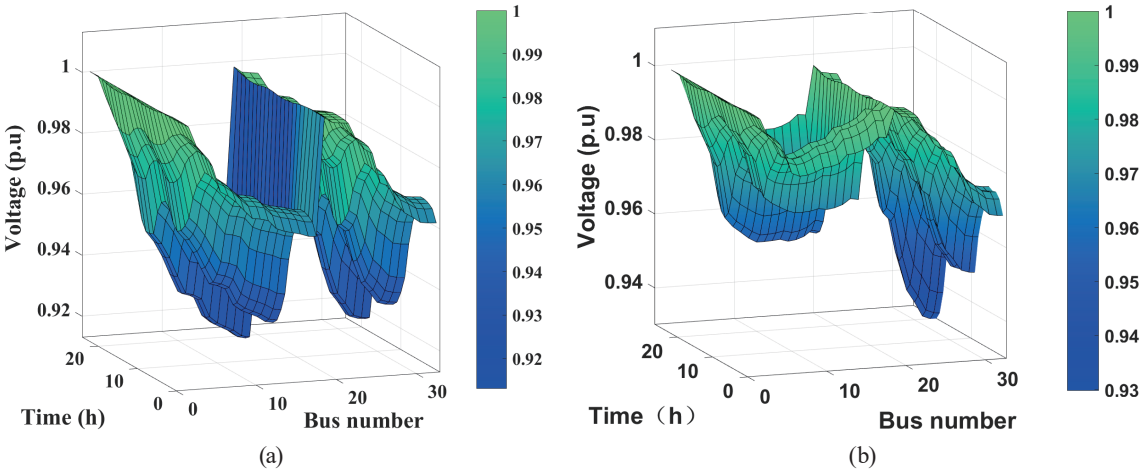

(a) (b)

Fig. 6. (Color online) Three-dimensional voltage distribution in the two cases. (a) Case 1 and (b) case 2.

5. Conclusions

In this study, a DG hierarchical planning model using ISCSO has been well established under wind and solar uncertainties. The major contributions of this study are as follows.

(1) The IEEE33 example verifies that the proposed model can effectively determine the scheme of DG access to the distribution network, significantly improve the system economy and power efficiency, and thus reduce network loss.
(2) By combining the initialization process, adaptive weight, and whale drop mutation, the ISCSO algorithm presents an excellent performance in convergence speed and accuracy compared with the other classical algorithms
(3) In the IEEE33 test system, the total annual cost is reduced by 13.1%, and the active network loss is reduced by 40.5%. This implies that the voltage deviation and network loss are reduced, thus ensuring the system voltage stability.

This study was focused on economic indicators without considering the impact of reactive power and voltage deviation. The issues regarding reactive power and voltage are proposed as topics of future work on the DG hierarchical planning model. In the future research, the voltage deviation can be used as one of the objective functions of the model to improve the power quality of the system. Additionally, the grid-connected distributed power supply may suffer from an island effect. Anti-islanding protection approaches can be developed and applied to the grid-connected line. Moreover, the suppression of the harmonic current generated in distributed generation networks might be another topic of future studies.

References

1 X. Song, Y. Wang, Z. Zhang, C. Shen, and F. Peña-Mora: Appl. Energy **281** (2021) 116142.
2 A. Norouzi, H. Shayeghi, and J. Olamaei: Energy Rep. **8** (2022) 12618.
3 L.-L. Li, J.-L. Lou, M.-L. Tseng, M. K. Lim, R. R. Tan: Expert Syst. Appl. **203** (2022) 117411.
4 A. Ahmed, M. F. Nadeem, A. T. Kiani, N. Ullah, M. A. Khan, and A. Mosavi: Energy Rep. **9** (2023) 1549.
5 A. S. Hassan, Y. Sun, and Z. Wang: Energy Rep. **6** (2020) 1581.
6 L.-L. Li, J.-L. Xiong, M.-L. Tseng, Z. Yan, and M. K. Lim: Expert Syst. Appl. **193** (2022) 116445.
7 B. Lin and C. Huang: Appl. Energy **337** (2023) 120891.
8 L.-L. Li, X.-D. Fan, M.-L. Tseng, K.-J. Wu, and K. Sethanan: Expert Syst. Appl. **237** (2024) 121406.
9 J. Zhong, Y. Cao, Y. Li, Y. Tan, Y. Peng, and L. Cao: Energy **224** (2021) 120179.
10 C. Pan, T. Jin, N. Li, G. Wang, X. Hou, and Y. Gu: Energy **270** (2023) 126846.
11 W. Xu, D. Zhou, X. Huang, B. Lou, and D. Liu: Appl. Energy **275** (2020) 115407.
12 A. Rathore and N.P. Patidar: J. Energy Storage **35** (2021) 102282.
13 Z. Moravej and A. Akhlaghi: Int. J. Electr. Power Energy Syst. **44** (2013) 672.
14 A. Uniyal and S. Sarangi: Electr. Power Syst. Res. **192** (2021) 106909.
15 R. Sellami, F. Sher, and R. Neji: Energy Rep. **8** (2022) 6960.
16 M. H. Ali, S. Kamel, M. H. Hassan, M. Tostado-Véliz, and H. M: Energy Rep. **8** (2022) 582.
17 M. Cikan and N. N. Cikan: Int. J. Electr. Power Energy Syst. **144** (2023) 108564.
18 T.E. Gümüş, S. Emiroglu, and M.A. Yalcin: Int. J. Electr. Power Energy Syst. **144** (2023) 108555.
19 F. Gao, C. Yuan, Z. Li, and S. Zhuang: Electr. Power Syst. Res. **214** (2023) 108914.
20 B. Sun, Y. Li, Y. Zeng, J. Chen, and J. Shi: Energy Rep. **8** (2022) 4209.
21 X. Zhao, H. Guo, P. Ding, W. Zhai, C. Liu, and C. Shen: Nano Energy **108** (2023) 108197.
22 M. Ma, B. He, N. Wang, and R. Shen: Sustainable Energy Technol. Assess. **53** (2022) 102678.
23 A. M. Ikotun, A. E. Ezugwu, L. Abualigah, B. Abuhaija, and J. Heming: Inf. Sci. **622** (2023) 178.